



Cite this: *RSC Adv.*, 2019, 9, 27780

Structural complexities and sodium-ion diffusion in the intercalates Na_xTiS_2 : move it, change it, re-diffract it†

Dennis Wiedemann, *^a Emmanuelle Suard ^b and Martin Lerch ^a

After momentary attention as potential battery materials during the 1980s, sodium titanium disulphides, like the whole Na–Ti–S system, have only been investigated in a slapdash fashion. While they pop up in current reviews on the very subject time and again, little is known about their actual crystal-structural features and sodium-ion diffusion within them. Herein, we present a short summary of literature on the Na–Ti–S system, a new synthesis route to $\text{Na}_{0.5}\text{TiS}_2\text{-}3R_1$, and results of high-temperature X-ray and neutron diffraction on this polytype, which is stable for medium sodium content. Based thereon, we propose a revision of the crystal structure reported in earlier literature (missed inversion symmetry). Analyses of framework topology, probability-density functions, and maps of the scattering-length density reconstructed using maximum-entropy methods (all derived from neutron diffraction) reveal a honeycomb-like conduction pattern with linear pathways between adjacent sodium positions; one-particle potentials indicate associated activation barriers of ca. 0.1 eV or less. These findings are complemented by elemental analyses and comments on the high-temperature polytype $\text{Na}_{0.9}\text{TiS}_2\text{-}2H$. Our study helps to get a grip on structural complexity in the intercalates Na_xTiS_2 , caused by the interplay of layer stacking and Na–Ti–vacancy ordering, and provides first experimental results on pathways and barriers of sodium-ion migration.

Received 23rd July 2019
 Accepted 25th August 2019

DOI: 10.1039/c9ra05690d

rsc.li/rsc-advances

Introduction

Layered lithium-ion conductors are a successful substance class for energy storage, e.g., in modern consumer electronics. Much effort has been put into research on their sodium congeners as possible high-voltage, low-cost alternatives—so far, to no commercial avail. Although alkali transition-metal dichalcogenides are not a recent focus, they pop up in current reviews time and again.¹ Probably as analogues of the once front-running lithium intercalates Li_xTiS_2 , the sodium compounds Na_xTiS_2 received some attention in the early to mid-1980s, leading to an overall manageable corpus of literature on the Na–Ti–S system. They have also sparked some commercial interest, manifested in patents, as thermoelectrics and auxiliary materials for cathodes in sodium-ion batteries.^{2,3}

As first Na–Ti–S compound, uncharacterised “ Na_2TiS_3 ” was reported in a process patent to have an X-ray pattern similar to the also uncharacterised “ Li_2TiS_3 ” and “ K_2TiS_3 ” in 1960.⁴ Five years later, Rüdorff described the first layered structure in the system and wrongly assigned it the NaHF_2 type [modern prototype according to the Inorganic Crystal Structure Database

(ICSD): $\text{CrOOH}(R\bar{3}m)$ —not yet aware of its hydrogen positions.⁵ Reliable sodium positions were not established before the first systematic study in 1971.⁶ Today, five kinds of Na–Ti–S compounds can be distinguished:

- The structure of the intercalates Na_xTiS_2 with $0 < x \leq 1$ consists of ${}^\infty[\text{TiS}_2]^{x-}$ sandwich layers with sodium ions in between. The compounds exist in four different structurally elucidated stacking variants: the polytypes $2H$, $3R_1$, $3R_2$, and $6H$ (see Table 1 and Fig. 1). With these materials, the remaining article is concerned.

- The excess-titanium compounds $\text{Na}_x\text{Ti}_{1+\delta}\text{S}_2$ with $0 < \delta \leq \frac{1}{3}$ and $0 < x \leq 1 - 3\delta$ contain additional titanium ions in intercalation layers, which hinder diffusion of the otherwise mobile sodium ions.¹⁴

- Contrary to its first assignment, $\text{Na}_2\text{TiS}_3 \equiv \text{Na}_{1.3}\text{Ti}_{0.6}\text{S}_2$ exhibits a structure homeotypic to Na_2SnS_3 , not K_2TiS_3 . At closer inspection, it crystallises in a sixfold superstructure of the $3R$ polytypes with an average structure akin to $\text{Na}_x\text{TiS}_2\text{-}3R_2$. It represents an OD structure with alternating pure sodium and mixed sodium-titanium layers, constituting a distorted NaCl homeotype.¹⁵ Upon heating, Na_2TiS_3 decomposes to $\text{NaTiS}_2\text{-}2H$ under oxidation of sulphide.⁸ The compound dubbed “ $3R'$ (II)- NaTiS_2 ” most probably is a sodium-deficient variant of Na_2TiS_3 .^{8,16}

- The electrochemically intercalated compounds Na_xTiS_3 contain sulphide as well as disulphide ions and are formed from TiS_3 via disulphide (instead of titanium) reduction and

^aTechnische Universität Berlin, Institut für Chemie, 10623 Berlin, Germany. E-mail: dennis.wiedemann@chem.tu-berlin.de

^bInstitut Laue-Langevin, 38042 Grenoble, France

† Electronic supplementary information (ESI) available: Details on X-ray diffraction, neutron diffraction, and corrections of the ICSD. See DOI: 10.1039/c9ra05690d



Table 1 Crystal-structurally characterised polytypes of Na_xTiS_2 ($0 < x \leq 1$) from literature

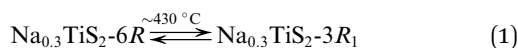
Polytype	$2H$	$3R_1$	$3R_2$	$6R$
Synonyms	$2H(I)$	$3R(I)$, phase I <i>b</i>	$3R(II)$, phase I <i>a</i>	$6R(I)$, phase II
Stability range ^a	High-temperature phase	$0.40(2) < x < 0.64(2)$ ($0.35 < x < 0.72$)	$0.75(2) < x \leq 1$ ($0.70 < x \leq 1$)	$0.15(2) < x < 0.25(2)$ ($0.10 < x < 0.33$)
Best characterised representative	$x = 1$ (ref. 7)	$x = 0.55$ (ref. 6)	$x = 1$ (ref. 6)	$x = 0.3$ (ref. 6 and 8)
Coordination polyhedron ⁹	Na [6 <i>p</i>] Ti [6 <i>o</i>]	[6 <i>p</i>] [6 <i>o</i>]	[6 <i>ap</i>] [6 <i>o</i>]	[6 <i>p</i>] [6 <i>o</i>]
Stage	1	1	1	2
Space-group type	$P6_3/mmc$	$R3m^c$	$R\bar{3}m$	$R\bar{3}m$
Structure prototype (ICSD)	NaTiS_2	CuCrSe_2^d	Delafossite- NaCrS_2	$\text{Ag}_{1.5}\text{Nb}_6\text{S}_{12}$
Delmas' notation ¹⁰	P2	P3	O3	O1–P3 ^e
Anion stacking	AABB	AABBCC	ABCABC	ABABBCBCCACA
Sodium-ion order ^b	Disordered over all voids	Ordered in half of the voids	Ordered in half of the voids	Disordered over all voids

^a Best values;¹¹ reported maximum extents in parentheses. ^b Within occupied sodium layers. ^c Corrected for a missed mirror plane,¹² originally given as $R3$. ^d Corrected in May 2019 (see Table S1),¹³ formerly ambiguously given as $\text{CuCrSe}_2\text{-AgCrSe}_2(R3m)$. ^e O1 layers are empty.

concomitant bond cleavage.¹⁷ They have neither been studied *ex situ* nor structurally characterised.

• Structurally complex Na_4TiS_4 has only been reported once in a book of poster abstracts. It is said to crystallise in the orthorhombic space group $Fdd2$ with $a = 38.49(2)$, $b = 59.36(3)$, $c = 7.033(2)$ Å, and $Z = 120$. The unit cell allegedly contains eight crystallographically independent TiS_4 tetrahedra, which are arranged in triple slabs parallel to (010).¹⁸

The polytype, which Na_xTiS_2 assumes, depends on x as well as on temperature. In the past, inconsistencies in reported stability ranges were discussed and *bona fide* best values were derived acknowledging synthetic (chemical *vs.* electrochemical intercalation) and analytical differences (diffraction patterns *vs.* discharge curves).¹¹ The only reported thermally induced phase transformations are the entropy-driven order–disorder transition for small x according to eqn (1) and the irreversible reconstitution of the (at ambient temperature metastable) $2H$ phase for large x following eqn (2).⁸ Transformations to the $2H$ form from either of the $3R$ polytypes were not observed and an irreversible transition between the latter was attributed to decomposition *via* sodium loss.



Ordering of sodium ions and vacancies was detected in electrochemically intercalated TiS_2 single crystals, where 2×2 , $2 \times \sqrt{3}$, and $\sqrt{3} \times \sqrt{3}$ superstructures may occur. For $x < 0.11$, a stage-3 compound with a $\sqrt{3} \times \sqrt{3}$ superstructure of a $3R$ phase containing sodium in trigonal-antiprismatic coordination was discovered but not conclusively characterised.^{19,20} The existence of such superstructures was later rationalised,²¹ comprehensively computed and explained.²²

Data on sodium-ion diffusion in Na_xTiS_2 are sparse. The chemical diffusivity at ambient temperature is specified as *ca.* 10^{-9} $\text{cm}^2 \text{s}^{-1}$ for $0.25 < x < 0.6$ (probably polytype $3R_1$).^{23,24} The much

higher value of 10^{-7} to 10^{-6} $\text{cm}^2 \text{s}^{-1}$ for $x < 0.45$, which was only reported once, remains questionable.²⁵ Unfortunately, migration barriers were merely computed for $\text{NaTiS}_2\text{-}3R_2$ (0.19 eV)²⁶ and a hypothetical Na_xTiS_2 with O1 coordination/layer sequence (1.02 eV).²⁷ Trigonal-antiprismatic coordination, as realised in the polytype $3R_2$, seems to hinder diffusion, so that diffusivities and migration barriers should be lower and higher in it, respectively, than in the other polytypes.²⁸

Our dealing with these materials is less inspired by prospective application as an ion conductor than by improving the grasp of ion diffusion in them and a comparing them to their lithium congeners. This is why, herein, we report on the revised crystal structure of and sodium-ion diffusion in $\text{Na}_{0.5}\text{TiS}_2\text{-}3R_1$ based on high-temperature neutron diffraction (ND). The study comprises

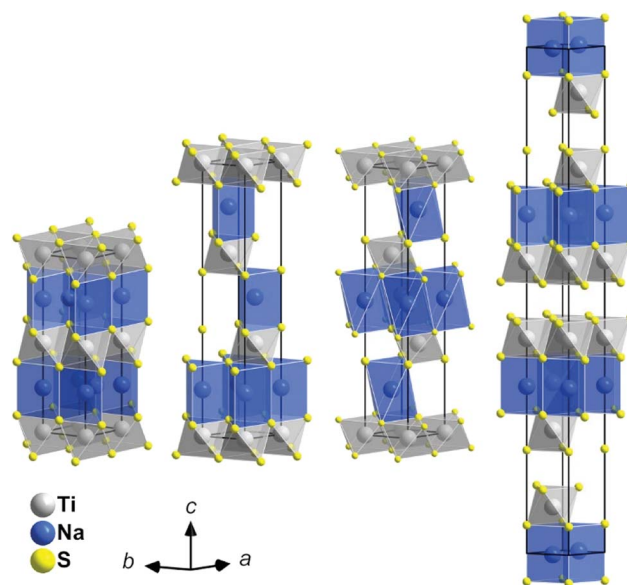


Fig. 1 Crystal structures of the Na_xTiS_2 polytypes; left to right: $2H$, $3R_1$, $3R_2$, and $6R$. Atoms are plotted with arbitrary radii, unit cells are depicted in black. Note: depending on x , sodium positions may not be fully occupied.



topological analyses, the visualisation of diffusion pathways using the probability-density function (PDF) and maps of the scattering-length density (SLD) reconstructed *via* maximum-entropy methods (MEM), as well as an evaluation of migration barriers using the effective one-particle potential (OPP). Results are complemented by temperature-dependent X-ray diffraction (XRD), elemental analyses, and comments on the related compound $\text{Na}_{0.9}\text{TiS}_2\cdot 2\text{H}_2\text{O}$.

Experimental

Analytical method

Hydrogen and sulphur contents were determined using a “Thermo Finnigan Flash EA 1112” analyser. Sodium was determined *via* optical emission spectroscopy with an inductively coupled plasma (ICP-OES) using a “Thermo Fisher Scientific iCAP 6300 Duo” evaluating the emission line at 589.5 nm.

The numbers of titanium ions per formula unit (with respect to sodium) were determined *via* wavelength-dispersive X-ray fluorescence (XRF) measurements on a “PANalytical Axios” spectrometer evaluating the intensities for the Na-K α and Ti-K α transitions. Samples were prepared from *ca.* 100 mg of analyte and 100 mg wax (Hoechst wax) performing uniaxial pressing (PerkinElmer hydraulic hand-press). Intensity ratios and sodium intensities were calibrated against linear regressions for three different mixtures of Na_2S and TiS_2 with $R(\text{Na}/\text{Ti}) = N(\text{Na}) \approx 0.4, 0.7,$ and 1.0 to account for instability/correlation of the titanium signal.

Synthetic procedures

Synthesis of $\text{TiS}_2\cdot 1\text{T}$. Polycrystalline $\text{TiS}_2\cdot 1\text{T}$ was prepared *via* direct synthesis from titanium (*ca.* 3.5 g, 1.00 eq.; Merck) and sulphur (2.10–2.20 eq.; Merck) in an evacuated silica ampoule. In a chamber furnace, the ampoule was heated to 400 °C with 25 °C h⁻¹ and held there for 40 h to achieve complete reaction. The temperature was then elevated to 600 °C and kept for 99 h, after which the oven was turned off to cool to room temperature. Residual sulphur was evaporated *in vacuo* at 160 °C. Identity and purity of the resulting greyish black powder with metallic lustre (typically *ca.* 8 g) were confirmed using XRD.

General synthesis of Na_xTiS_2 . $\text{TiS}_2\cdot 1\text{T}$ (*ca.* 3.5 g, 1.00 eq.) and Na_2S (0.25 or 0.45 eq.; Sigma-Aldrich, $\geq 97\%$) were ground together in an agate mortar. The mixture was placed in a corundum crucible, which was subsequently heated to 700 °C with a rate of 400 °C h⁻¹ in a tube furnace under H_2S atmosphere (99.5%, Air Liquide), kept at that temperature for 2 h, and then cooled to ambient temperature with a rate of 200 °C h⁻¹. The product was removed in a dinitrogen counter-flow and stored under argon. The reaction afforded Na_xTiS_2 (yield: *ca.* 99%) as greyish black, microcrystalline powder with a metallic lustre for high sodium content.

Found: H, 1.0(1); Na, 8.8(1); S, 48(1); $N(\text{Ti}) = 1.0(2)$. Calc. for $\text{Na}_{0.5}\text{S}_2\text{Ti}\cdot\frac{1}{2}\text{H}_2\text{O}$: H, 0.8; Na, 8.7; S, 48.4%; $N(\text{Ti}) = 1.0$.

X-ray diffraction

Measurements for phase identification and Rietveld refinement were carried out at ambient temperature on a “PANalytical X'Pert PRO MPD” diffractometer equipped with a “PIXcel”

detector using nickel-filtered Cu-K α radiation in Bragg–Brentano (θ – θ) geometry (see Fig. S1† for details). Temperature-dependent diffractograms were recorded in dinitrogen atmosphere on a “Rigaku SmartLab 3 kW” system using nickel-filtered Cu-K α radiation.

Neutron diffraction

Measurement was carried out at Institut Laue-Langevin (ILL) using the high-resolution two-axis diffractometer D2B with Ge(335)-monochromated constant-wavelength radiation ($\lambda = 1.594$ Å) in Debye–Scherrer geometry.^{29,30} Compacted powder samples were mounted in a vacuum high-temperature furnace inside a vanadium can ($d = 13.9$ mm, $h = 49.8$ mm). Measurements were carried out at ambient temperature, 300, 600, and 700 °C. Data were recorded with an array of 128 ³He tubes (height: 300 mm), yielding a final range of $0.10^\circ \leq 2\theta \leq 159.90^\circ$ with $\Delta(2\theta) = 0.05^\circ$. Initial Le-Bail fits and following Rietveld refinements were carried out using JANA2006.³¹ Neutron data were analytically corrected for absorption (cylindrical sample) and stripped of the irregular onset below 6.5° and, if necessary, cut-off reflections above 155° . Peak profiles were fitted with a pseudo-Voigt function using the Thompson–Cox–Hastings approach (Gaussian parameters $U, V,$ and W ; Lorentzian parameter X). A zero-shift correction and an asymmetry correction according to Howard were applied.³² The background was modelled using ten Legendre polynomials interpolating between manually defined points. Relatively weak reflections of a by-phase assuming the space-group type $Fm\bar{3}m$ (probably steel from the sample environment) were treated with an appropriate Le-Bail fit (separate profile parameters).

As a starting point for Rietveld refinement, an atomic model of $\text{Na}_{0.55}\text{TiS}_2$ was imported from the ICSD and adjusted to reflect the actual cell content and symmetry.³³ Anisotropic displacement parameters were refined for all atoms except for Ti1 at 18 °C, the very small displacement of which had to be constrained to isotropy to yield a positive-definite value. For Na1 at 600 and 700 °C, anharmonic displacement was observed. Terms up to the fourth order were tested and only kept in refinement if they were significant ($|C_{ijk}| \geq 3\sigma[C_{ijk}]$) and led to a significant drop in R values. Thus, two additional unique parameters $C_{111}(\text{Na1})$ and $C_{333}(\text{Na1})$ were refined. Towards the end of refinement, $z(\text{Na1})$ was found to be within a 3σ interval of $\frac{1}{6}$ (coplanarity of sodium ions) and was fixed at this value, yielding slightly better residuals despite one free parameter less.

Structure graphics were produced using Diamond 4.5 and VESTA.^{34,35} Refinement results are summarized in Table 2. Diffraction datasets are available in the ILL repository.³⁶ CSD 1942255 to 1942259 contain the supplementary crystallographic data for this paper; these data can be obtained free of charge from FIZ Karlsruhe *via* <https://www.ccdc.cam.ac.uk/structures>.

Procrystal void analysis

Procrystal voids in the TiS_2^{x-} substructures were analysed using CrystalExplorer 17.5 with default options.³⁷ Models were based on the revised room-temperature structure of $\text{Na}_{0.5}\text{TiS}_2\cdot 3\text{R}_1$ and



Table 2 Details of crystal structures and refinements on neutron diffraction data

Formula	$\text{Na}_{0.5}\text{TiS}_2$			
$M_r/\text{g mol}^{-1}$	123.48			
$\theta/^\circ\text{C}$	18	300	600	700
Space group	$R\bar{3}m$			
$a/\text{\AA}$	3.43840(8)	3.45878(5)	3.47973(6)	3.48717(7)
$c/\text{\AA}$	21.0431(6)	21.2010(5)	21.3240(7)	21.3635(8)
$V/\text{\AA}^{-3}$	215.453(14)	219.651(9)	223.610(12)	224.983(14)
Z	3	3	3	3
Meas./obs. ^a reflections	73/69	79/74	79/71	79/71
R_p	0.0268	0.0195	0.0178	0.0177
wR_p^b	0.0359	0.0257	0.0232	0.0230
R_{exp}	0.0176	0.0176	0.0175	0.0175
R_F	0.0333	0.0320	0.0352	0.0414
R_I^a	0.0520	0.0462	0.0438	0.0464

^a $I > 3\sigma(I)$. ^b $w = 1/[\sigma^2(I) + (0.01I)^2]$.

structures of $\text{NaTiS}_2\text{-}2H$, $\text{NaTiS}_2\text{-}3R_2$, and $\text{Na}_{0.3}\text{TiS}_2\text{-}6R$ from the ICSD.³³ Lower bounds for contiguous void networks were found by successively altering the procrystal density in steps of $\Delta\rho_{\text{pro}} = 0.0001$ a.u.

MEM reconstruction

Dysnomia 1.0 was used for MEM-reconstruction of SLDs from final structure factors as put out by JANA2006.³⁸ The unit cell was divided into $96 \times 96 \times 588$ voxels. Starting from a uniform intensity prior, the limited-memory Broyden–Fletcher–Goldfarb–Shanno (L-BFGS) algorithm³⁹ was employed with uncertainties augmented by $E = 0.5$ and relative weights set to $\lambda_2 = 1$, $\lambda_n = 0$ for $n \geq 4$ to avoid overfitting. Final R_F/wR_F were 0.0342/0.0305 and 0.0376/0.0328 for data acquired at 600 and 700 °C, respectively.

OPP calculation

Sodium OPPs were calculated from PDFs as well as from MEM-reconstructed SLDs using CalcOPP 2.0.1.⁴⁰ In the latter case, the maximal positive SLD found within the sodium layer was set to represent a potential energy of $V = 0$. For error estimation on PDF-derived data, the Monte-Carlo routines implemented in JANA2006 were employed (10 000 iterations, final accuracy < 1%).

Results and discussion

Synthesis and structure

The intercalates Na_xTiS_2 can be synthesized from the binary sulphides in a H_2S feed. At 700 °C, ca. 3–4% of H_2S decompose into H_2 and S_n .⁴¹ This creates a mildly reductive atmosphere that acts according to eqn (3).



Compounds of this type are very hygroscopic and may reversibly co-intercalate up to two equivalents of water per formula unit without degradation.^{42,43} Elemental analyses show that even short handling in air is enough to effect absorption of

ca. half an equivalent of water (no significant difference between stored samples with and without neutron diffractometry was observed). At the elevated temperatures examined herein, however, the samples dehydrate completely.

During refinement of the initial model derived from $\text{Na}_{0.55}\text{TiS}_2\text{-}3R_1$ against ND data, occupation of a second sodium position at $(\frac{2}{3}, \frac{1}{3}, \sim 0.17)$, strong correlation of the sulphide ions' z coordinates, and refinement instability occurred. A closer look at the structures in the hitherto assigned space group $R3m$ and its supergroup $R\bar{3}m$ reveals the following differences: the two unique sulphide positions with $z = 0.39$ and 0.60 in the former correspond to a single one with $z = 0.40$ in the latter (mismatch $\Delta z = 0.01$). The two nearly equally occupied sodium positions with $z = 0.17$ correspond to a single position that has to be at $z = \frac{1}{6}$ to warrant a coplanar arrangement (mismatch $\Delta z = 0.0$). Refinement in $R\bar{3}m$ solved the initial problems (see Fig. 2 for exemplary and Fig. S4–S6† for remaining diffractograms). We found no hint at symmetry lowering at any temperature. While $\text{Na}_{0.55}\text{TiS}_2$ as synthesised by Rouxel *et al.*⁶ might represent an ordered variant, we assume a case of missed symmetry because of the following reasons: due to the perfect overlap of all reflections in $R3m$ that are symmetry equivalent in $R\bar{3}m$, only

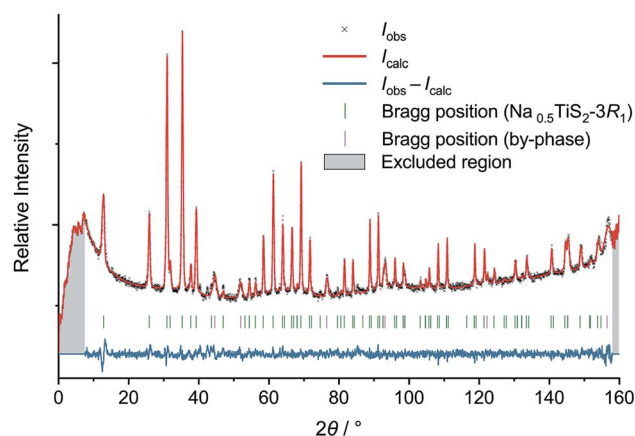


Fig. 2 Neutron diffractogram of $\text{Na}_{0.5}\text{TiS}_2\text{-}3R_1$ (revised structure) at 700 °C with results of Rietveld refinement.



ever-so-subtle intensity differences distinguish one from the other (see Fig. S2†). For $3R_1$ -isotypic $K_{0.6}VS_2$, Bronsema and Wiegers recognised the same problem and could not resolve it *via* X-ray powder diffraction.⁴⁴ Furthermore, both sodium positions in $R3m$ are crystal-chemically nearly identical and should not give rise to ordering. We thus conclude that the published structure is to be revised.†

Temperature-dependent XRD shows that, on heating, a previously stored $Na_{0.5}TiS_2 \cdot 3R_1$ sample loses co-intercalated water up to 100 °C (see Fig. 3, characteristic reflection at *ca.* 10°). No phase change akin to the $1T$ - $3R$ transformation§ in the lighter homologue $Li_{0.7}TiS_2$ occurs.⁴⁵ In dinitrogen atmosphere above 550 °C, decomposition starts (slight reflection-positional shift to higher angles, degradation of intensities, additional small reflections) under concomitant sulphur formation (found in the reaction chamber). While the absence of phase transitions is confirmed by ND, the sample has proven to be stable in a vanadium can surrounded by vacuum up to at least 700 °C. Cell dimensions lie in the range expected for $x = 0.5$ at ambient temperature and evolve in a roughly linear fashion during heating (*cf.* Fig. S7†).⁴⁶ The latter also holds for the equivalent displacement parameters of the titanium and sulphide ions, whereas the one of the sodium ion starts at a value five to six times as large and grows disproportionately (see Fig. S8 and S9†). This is due to supposedly static disorder at room temperature and the onset of anharmonic dynamics (*i.e.*, ion diffusion) between 300 and 600 °C.

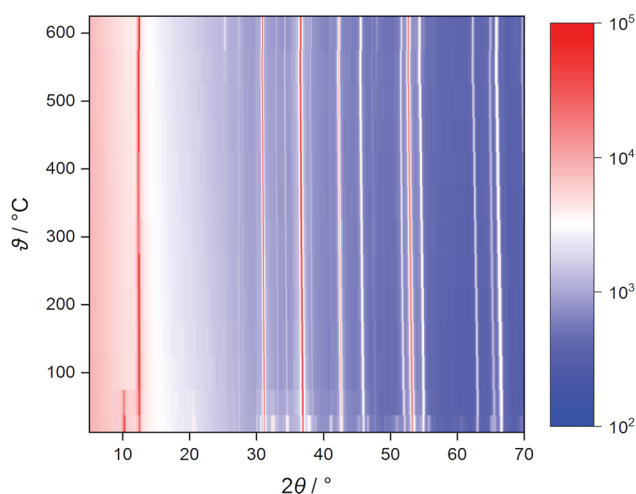


Fig. 3 Heat map of uncorrected temperature-dependent X-ray diffractograms of $Na_{0.5}TiS_2 \cdot 3R_1$ in dinitrogen atmosphere. The colouring is based on raw counts; the scale is logarithmic.

† The previous assignment of the structure type “ $CuCrSe_2$ - $AgCrSe_2(R3m)$ ” to $Na_{0.5}TiS_2 \cdot 3R_1$ complicated a comparison to other structures: several isopointal but alloconfigurational structures were assigned this ill-defined type. It was split correctly in the course of this work (see Table S2†), the result being incorporated in the ICSD since May 2019.¹³

§ The compounds $Li_xTiS_2 \cdot 3R$ are isotypic to the high-alkali polytype $Na_xTiS_2 \cdot 3R_2$, not $Na_xTiS_2 \cdot 3R_1$.

Sodium diffusion pathways

We will describe the methods used herein very briefly. A more detailed overview has already been published.⁴⁷ The pathways refer to thermally activated ion diffusion at temperatures high enough to warrant ample ion mobility.

Procrystal void analysis. The procrystal void analysis is a fast tool to find the most probable pathways for ion diffusion and to compare compounds, of which only the structure is known.⁴⁸ Leaving out the mobile (in this case, sodium) ions, the method constructs the remaining static framework as a superposition of diffuse spherical electron densities centred at the atomic positions—the so-called procrystal density ρ_{pro} . The latter contains voids that are characterised by an isovalue of a surface enclosing them: the lower the value, the “emptier” the void, the better its suitability for containing/conducting an ion.

The low and comparable isovalues, at which the voids in the polytypes $2H$,¶ $3R_1$ (our revised structure), and $6R$ form contiguous paths, indicate that they are similarly well-suited sodium-ion conductors (see Fig. 4). The framework voids are located at the partly occupied sodium positions and connect to a honeycomb-like conduction pattern. The voids in the $3R_2$

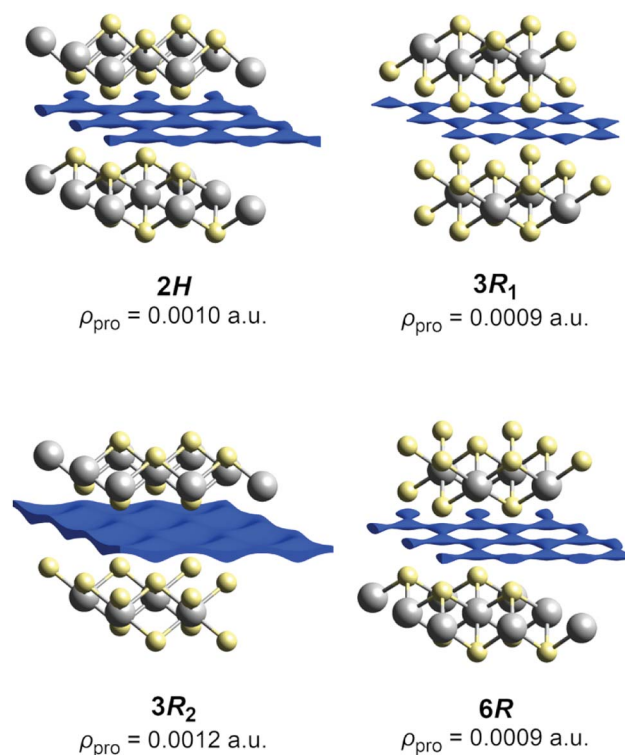


Fig. 4 Procrystal void surfaces (blue) in the sodium layers of the TiS_2^{x-} frameworks for different polytypes. Atoms are plotted with covalent radii (grey: titanium, yellow: sulphide ions). The depicted isovalue is the minimum for a contiguous surface.

¶ *Caveat:* There had been a transcription error in the former ICSD record that was corrected in 2018.



structure also arrange in a honeycomb-like fashion and give no hint at any reason for an ordered occupation of half of them (like the current structural model suggests). The voids connect at a significantly higher isovalue to a carpet-like pattern, which suggests that this polytype is a worse and more isotropic sodium-ion conductor.

Probability-density function. The PDF of an atom at a point in space describes the probability of finding said atom displaced from its equilibrium position to said point. In the case of harmonic displacement, the depiction of the PDF as isosurface leads to the well-known spheres (isotropic) or ellipsoids (anisotropic). In the anharmonic case, however, forms that are more complex ensue. Because of this, a superposition of the PDFs of several atoms, called a joint probability-density function (JPDF), allows the visualisation of diffusion pathways.

In the case at hand, the sodium ions are displaced along linear pathways between adjacent sodium positions at both relevant temperatures (*cf.* the similar isosurfaces in Fig. 5). In this way, the honeycomb-like conduction pattern predicted by procrystal void analysis is indeed experimentally reproduced.

MEM-reconstructed scattering-length density. To rule out bias, we have also inspected maps of the MEM-reconstructed SLD, which do not rely on modelling atomic displacement. In comparison to maps directly Fourier-transformed from the structure factors, they are deprived of artefacts and show a flatter distribution of noise. The maps show that our PDF model is indeed accurate and reproduces even finer features of the positive sodium-associated SLD (see Fig. 6).

In the lighter but more alkali-rich congeners $\text{Li}_x\text{TiS}_2\text{-}3R_1$ ($x = 0.7, 0.9$), preferred ion pathways were found between adjacent lithium positions.⁴⁹ Because of their ordering, however, they correspond to second-neighbours in disordered $\text{Na}_{0.5}\text{TiS}_2\text{-}3R_1$. As a result, the pathways are not directly comparable. It is noteworthy that, in contrast to $\text{Li}_x\text{TiS}_2\text{-}3R$, we have not found a significant deviation from coplanarity. We attribute this to the differences in coordination polyhedra (trigonal antiprism *vs.* prism) and spatial

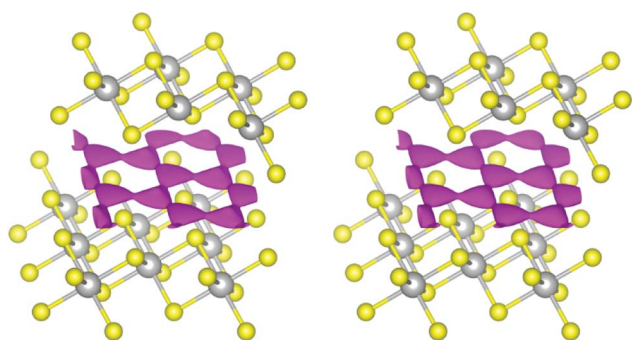


Fig. 5 Joint sodium-PDF isosurface of 0.09 \AA^{-3} (pink) in $\text{Na}_{0.5}\text{TiS}_2\text{-}3R_1$ at $600 \text{ }^\circ\text{C}$ (left) and $700 \text{ }^\circ\text{C}$ (right). Atoms are plotted with covalent radii (grey: titanium, yellow: sulphide ions).

arrangement (interlayer spacing larger by $\Delta d \approx 0.96 \text{ \AA}$, while ionic diameter only larger by $2\Delta r = 0.52 \text{ \AA}$ (ref. 50) for the sodium compound).

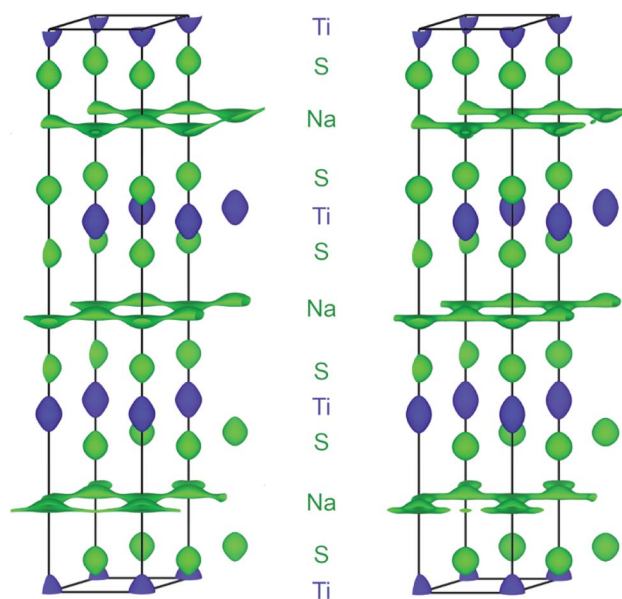


Fig. 6 SLD isosurface of $\pm 0.5 \text{ fm \AA}^{-3}$ (green: positive, blue: negative) in $\text{Na}_{0.5}\text{TiS}_2\text{-}3R_1$ at $600 \text{ }^\circ\text{C}$ (left) and $700 \text{ }^\circ\text{C}$ (right) with view roughly along a^* . Atomic layers are assigned to elements, unit cells are depicted in black.

Migration barriers

For the estimation of the migration energy barrier associated with the found path, we calculated the OPP, which represents the energy landscape experienced by a mobile sodium ion (approximated as an Einstein oscillator that is subject to Boltzmann statistics at the classical limit). The activation energy of the migration (not comprising the defect formation energy) is the OPP at the bottleneck position, *i.e.*, the position of lowest probability along the pathway.

The calculation of OPPs from ND-derived PDFs is fairly established,⁵¹ but direct derivations from MEM-reconstructed SLDs without any further refinement are scarce.⁵² The latter is only warranted if an SLD shares basic characteristics of a probability density. Mathematically speaking, a PDF has to be non-negative, Lebesgue-integrable, and normalized to an integral of unity over the whole space. To give a reason for using the direct approach nonetheless, the following points address these issues not in a rigorous but hand-waving way:

- The OPP calculation deals with ratios of input values. Only the non-negative ones are taken into account.
- Numerically sampled SLDs are Lebesgue-integrable.
- For ratios of input values, normalization is unnecessary (the normalizing constant cancels).

Furthermore, the adequacy of the results is ensured by only taking the SLD solely caused by sodium ions (*i.e.*, within the sodium layers) into account.

In agreement with crystal-chemical assumptions, we found the bottleneck of migration at $\frac{1}{3}, \frac{1}{6}, \frac{1}{6}$ —in the middle of a straight line between adjacent sodium positions. The OPPs at this point are summarized in Table 3. Generally, the activation energy does not depend on the temperature as long as only a single



migration mechanism is concerned and the structure is stable. For this method, however, this holds only if diffusion is fully activated because the migrating ions themselves are the probe for the potential. This is why slightly lower activation barriers are often found for higher temperatures—as is the case here for the central values—and are thought to be more reliable. Nevertheless, the PDF-derived energies are equal within 1σ . Currently, there is no computational way to estimate the errors on SLD-derived values. Judging by the uncertainties of the PDF-derived barriers, however, the central values are significantly lower, but of the same magnitude. As this is the first study employing both methods, it remains yet unknown if the deviation is systematic. It is, *e.g.*, possible that a restricted set of parameters models parts of the SLD imperfectly (thereby modelling a too low probability density resulting in a too high OPP) or that the SLD-derived OPP carries a considerable error.

The topography of the OPP landscape, on the other hand, is similar irrespective of temperature or calculation method (see Fig. 7). As temperature rises, the potential becomes flatter and gives access to a larger area (*cf.* Fig. 7a/b), but the basic shape is preserved. As the sodium PDF reproduces the features of the SLD (*vide supra*), the landscapes derived from both resemble each other (*cf.* Fig. 7c/d). The smaller volume enclosed by the same isosurface, however, shows that the SLD-derived OPP is steeper, therefore stemming from a more localised distribution.

The experimental barriers are lower than computed for defective $\text{NaTiS}_2\text{-}3R_2$ (0.19 eV)²⁶ and measured for $\text{Li}_{0.7}\text{TiS}_2\text{-}3R$ (*ca.* 0.5 eV).⁴⁹ Procrystal void analysis already led us to expect that these homeotypic (by alkali occupation) structures be detrimental to alkali-ion conduction (*vide supra*). In addition, the lower number of vacancies (higher alkali content) in the latter hinders migration.⁴⁹ For $\text{Na}_{0.5}\text{TiS}_2\text{-}3R_1$, low activation barriers corroborate its role as a good sodium-ion conductor. Although a model all-solid-state sodium-ion battery using a Na_xTiS_2 electrode has been realized,⁵³ problems with reactivity, phase transformations upon de-/intercalation, and mediocre cyclability seem to prohibit its effective use therein.⁵⁴

Remarks on “ $\text{Na}_{0.9}\text{TiS}_2\text{-}2H$ ”

Our endeavour to explore also the more sodium-rich $\text{Na}_{0.9}\text{TiS}_2\text{-}2H$ was hindered by synthesis problems. While XRD for phase identification and ND seemed to indicate a single-phase product of the desired polytype, closer inspection (see Fig. S3†) revealed at least two similar phases, possibly with a more complex (OD) structure. Because of the broader reflections in ND, we found no way of separating the contributions of

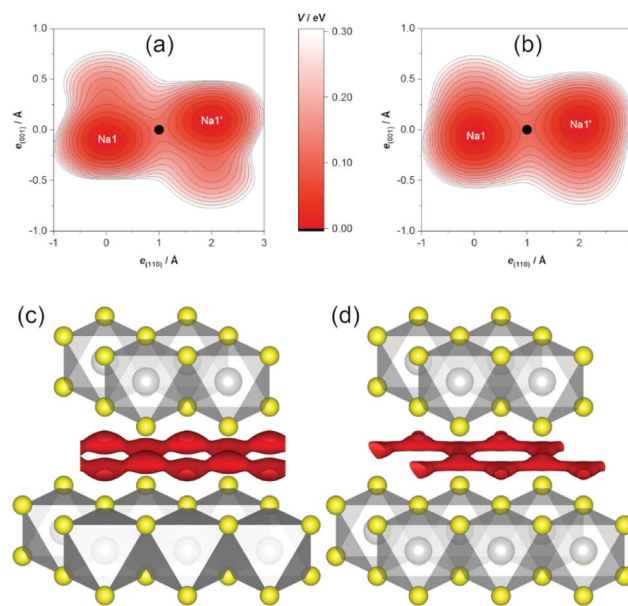


Fig. 7 Sodium OPP V in $\text{Na}_{0.5}\text{TiS}_2\text{-}3R_1$. Top: Contour plot of PDF-derived OPP within a plane containing two adjacent sodium ions at (a) 600 °C and (b) 700 °C (origin at Na1, bottleneck as black dot, contours: from $V_0 = 0$ on with $\Delta V = 0.025$ eV). Bottom: Isosurface plots of (c) PDF-derived and (d) SLD-derived OPP of $V = 0.15$ eV at 700 °C (atoms as with covalent radii; grey: titanium, yellow: sulphide ions, red: OPP isosurface).

different phases. A refined (unphysical) single-phase model averaging over all phases was at odds with elemental analysis: The former found only *ca.* 0.5 sodium ions per formula unit at the crystallographic positions (no significant positive residual SLD) while the latter conformed to the target composition.

Furthermore, we found a strong preferred orientation in (001) that agrees well with the plate-like visual appearance of the crystallites in the sample. In a temperature-dependent XRD experiment, we observed the $2H$ -like structure over the whole stability range. No signs of a transformation into a supposedly stable $3R_2$ -like structure showed above 300 °C, even when heating for a longer time.

Conclusions

We synthesised the intercalate $\text{Na}_{0.5}\text{TiS}_2\text{-}3R_1$ from sodium and titanium sulphide in a mildly reducing H_2S atmosphere. Our ND and XRD experiments showed that its structure, as reported in the literature, has to be revised: $\text{Na}_{0.5}\text{TiS}_2\text{-}3R_1$ assumes the space-group type $R\bar{3}m$ (not $R3m$) with disordered (not ordered) sodium ions and one (not two) crystallographically independent sulphide position. Up to *ca.* 100 °C, the compound reversibly co-intercalates half an equivalent of water. It is stable with respect to phase transformations up to its decomposition temperature.

Sodium-ion diffusion manifests in anharmonic displacement at 600 and 700 °C. In agreement with expectations from topological analysis of the static TiS_2^{x-} framework, maps of the MEM-reconstructed SLD and modelled PDFs show a honeycomb-like conduction pattern with linear almost in-plane

Table 3 Activation energies (in eV) of sodium-ion migration in $\text{Na}_{0.5}\text{TiS}_2\text{-}3R_1$

Calculation	At 600 °C	At 700 °C
From displacement-derived PDF	0.114(7)	0.108(8)
From MEM-reconstructed SLD	0.086	0.070



pathways between adjacent (partly occupied) sodium positions. The bottlenecks of migration are found at the midpoint of said pathways. The associated OPPs at 700 °C indicate low activation barriers of 0.108(8) eV or even 0.070 eV (derived from PDF or SLD, respectively).

Unfortunately, we could not complement these findings with data for $\text{Na}_{0.9}\text{TiS}_2\text{-}2H$. We presume that our synthesis method led to segregation into at least two $2H$ -like phases—one with lower, one with higher sodium content. Possibly, these are closely related to Na_2TiS_3 with its OD structure. Bouwmeester *et al.* had already found such by-phases (re-)forming during high- to mid-temperature syntheses *ex elementis* with high sodium load.⁸ The potential of arranging

- pure sodium layers (*e.g.*, in NaTiS_2), their defective (*e.g.*, in Na_xTiS_2 with $x < 1$), titanium-mixed (*e.g.*, in Na_2TiS_3), or even as-well-as variants (*e.g.*, in $\text{Na}_x\text{Ti}_{1+\delta}\text{S}_2$ with $x < 1 - 3\delta$)
 - with their sodium, titanium, and vacancy positions ordered or unordered within one layer
 - in an ordered or unordered stacking sequence
- accounts for compelling structural complexity in layered sodium titanium sulphides. This is particularly pronounced at the fringes of very high or very low alkali content and makes further exploration, especially of the interplay between sodium mobility and structural disorder, worthwhile.

Conflicts of interest

There are no conflicts to declare.

Acknowledgements

Financial support by the Deutsche Forschungsgemeinschaft (SPP 1613, LE 781/13-2) is gratefully acknowledged. The article processing charge was covered by FILL2030, a European Union project within the European Commission's Research and Innovation programme Horizon 2020 under grant agreement no. 731096. We thank Dr Stefan Berendts for XRF analyses and temperature-dependent XRD, Dr Suliman Nakhil for the synthesis of $\text{TiS}_2\text{-}1T$, Ms Juana Krone for sulphur and hydrogen determination, and Ms Iris Pieper for sodium determination.

Notes and references

- 1 J.-Y. Hwang, S.-T. Myung and Y.-K. Sun, *Chem. Soc. Rev.*, 2017, **46**, 3529–3614.
- 2 H. Imai, Y. Shimakawa, T. Mako and Y. Kubo, *JP Pat.*, 2002-270907, 2002.
- 3 R. Zhang, F. Mizuno, C. Ling, M. S. Whittingham, R. Zhang and Z. Chen, *US Pat.*, 20160365577, 2016.
- 4 A. Clearfield, *US Pat.*, 3148998, 1960.
- 5 W. Rüdorff, *Chimia*, 1965, **19**, 489–499.
- 6 J. Rouxel, M. Danot and J. Bichon, *Bull. Soc. Chim. Fr.*, 1971, 3930–3935.
- 7 R. J. Haange, A. J. A. Bos-Alberink and G. A. Wiegers, *Ann. Chim. Sci. Mater.*, 1978, **3**, 201–207.
- 8 H. J. M. Bouwmeester, E. J. P. Dekker, K. D. Bronsema, R. J. Haange and G. A. Wiegers, *Rev. Chim. Miner.*, 1982, **19**, 333–342.
- 9 J. Lima-de-Faria, E. Hellner, F. Liebau, E. Makovicky and E. Parthé, *Acta Crystallogr., Sect. A: Found. Crystallogr.*, 1990, **46**, 1–11.
- 10 C. Delmas, C. Fouassier and P. Hagenmuller, *Physica B+C*, 1980, **99**, 81–85.
- 11 P. Molinier, L. Trichet, J. Rouxel, C. Berthier, Y. Chabre and P. Segransan, *J. Phys. Chem. Solids*, 1984, **45**, 105–112.
- 12 K. Cenoz, L. M. Gelato, M. Penzo and E. Parthé, *Acta Crystallogr., Sect. B: Struct. Sci.*, 1991, **47**, 433–439.
- 13 R. Hinek, personal communication.
- 14 D. A. Winn, J. M. Shemilt and B. C. H. Steele, *Mater. Res. Bull.*, 1976, **11**, 559–566.
- 15 P. Colombet, M. Danot, J.-C. Jumas and É. Philippot, *C. R. Séances Acad. Sci., Sér. C*, 1978, **287**, 411–414.
- 16 W. Mark, O. Lindqvist, J.-C. Jumas and É. Philippot, *Acta Crystallogr., Sect. B: Struct. Crystallogr. Cryst. Chem.*, 1974, **30**, 2620–2628.
- 17 M. Zanini, J. L. Shaw and G. J. Tennenhouse, *J. Electrochem. Soc.*, 1981, **128**, 1647–1650.
- 18 K. O. Klepp, *Z. Kristallogr. Suppl.*, 1995, **9**, 188.
- 19 T. Hibma, *Physica B+C*, 1980, **99**, 136–140.
- 20 T. Hibma, *J. Solid State Chem.*, 1980, **34**, 97–106.
- 21 Q.-g. Song, X.-z. Cong, Q.-j. Zhang, W.-l. Mo and Z.-h. Dai, *Wuli Xuebao*, 2000, **49**, 2011–2016.
- 22 J. Vinčevićiūtė, M. D. Radin and A. Van der Ven, *Chem. Mater.*, 2016, **28**, 8640–8650.
- 23 K. M. Abraham, *Solid State Ionics*, 1982, **7**, 199–212.
- 24 W. B. Johnson and W. L. Worrell, *Synth. Met.*, 1982, **4**, 225–248.
- 25 B. A. Marmaduke and L. F. Donaghey, *Proc. Intersoc. Energy Convers. Eng. Conf.*, 1976, **1**, 467–470.
- 26 X. Zhang, Z. Zhang, S. Yao, A. Chen, X. Zhao and Z. Zhou, *npj Comput. Mater.*, 2018, **4**, 13.
- 27 S. N. Li, J. B. Liu and B. X. Liu, *J. Power Sources*, 2016, **320**, 322–331.
- 28 B. G. Silbernagel and M. S. Whittingham, *Mater. Res. Bull.*, 1976, **11**, 29–36.
- 29 A. W. Hewat, *Mater. Sci. Forum*, 1986, **9**, 69–80.
- 30 E. Suard and A. Hewat, *Neutron News*, 2001, **12**, 30–33.
- 31 V. Petříček, M. Dušek and L. Palatinus, *Z. Kristallogr. - Cryst. Mater.*, 2014, **229**, 345–352.
- 32 C. J. Howard, *J. Appl. Crystallogr.*, 1982, **15**, 615–620.
- 33 G. Bergerhoff and I. D. Brown, in *Crystallographic Databases*, ed. F. H. Allen, G. Bergerhoff and R. Sievers, International Union of Crystallography, Chester, U.K., 1987, ch. 2.2, pp. 77–95.
- 34 K. Brandenburg, *Diamond 4.5*, Crystal Impact – H. Putz & K. Brandenburg GbR, Bonn, Germany, 2018.
- 35 K. Momma and F. Izumi, *J. Appl. Crystallogr.*, 2011, **44**, 1272–1276.
- 36 M. Lerch, E. Suard and D. Wiedemann, *Pathways of Sodium-Ion Diffusion in Na_xTiS_2 ($x = 0.5, 0.9$)*, 2017, accessed June 2019, DOI: 10.5291/ill-data.5-21-1106.



- 37 M. J. Turner, J. J. McKinnon, S. K. Wolff, D. J. Grimwood, P. R. Spackman, D. Jayatilaka and M. A. Spackman, *CrystalExplorer 17.5*, University of Western Australia, Perth, Australia, 2017.
- 38 K. Momma, T. Ikeda, A. A. Belik and F. Izumi, *Powder Diffr.*, 2013, **28**, 184–193.
- 39 J. Nocedal, *Math. Comput.*, 1980, **35**, 773–782.
- 40 D. Wiedemann, *CalcOPP 2.0.1*, Technische Universität Berlin, Berlin, Germany, 2019, DOI: 10.5281/zenodo.2530345.
- 41 V. E. Kaloidas and N. G. Papayannakos, *Int. J. Hydrogen Energy*, 1987, **12**, 403–409.
- 42 R. Schöllhorn and A. Weiss, *Z. Naturforsch., B: Anorg. Chem., Org. Chem.*, 1973, **28**, 711–715.
- 43 S. N. Patel and A. A. Balchin, *J. Mater. Sci.*, 1985, **20**, 917–921.
- 44 K. D. Bronsema and G. A. Wiegers, *Mater. Res. Bull.*, 1987, **22**, 1073–1080.
- 45 D. Wiedemann, S. Nakhal, A. Senyshyn, T. Bredow and M. Lerch, *Z. Phys. Chem.*, 2015, **229**, 1275–1288.
- 46 J. Rouxel, in *Intercalated Layered Materials*, ed. F. Lévy, D. Reidel Publishing, Dordrecht, Netherlands, 1979, pp. 201–250.
- 47 D. Wiedemann, M. M. Islam, T. Bredow and M. Lerch, *Z. Phys. Chem.*, 2017, **231**, 1279–1302.
- 48 M. J. Turner, J. J. McKinnon, D. Jayatilaka and M. A. Spackman, *CrystEngComm*, 2011, **13**, 1804–1813.
- 49 D. Wiedemann, M. M. Islam, S. Nakhal, A. Senyshyn, T. Bredow and M. Lerch, *J. Phys. Chem. C*, 2015, **119**, 11370–11381.
- 50 R. D. Shannon, *Acta Crystallogr., Sect. A: Cryst. Phys., Diffr., Theor. Gen. Crystallogr.*, 1976, **32**, 751–767.
- 51 H. Boysen, *Z. Kristallogr.*, 2003, **218**, 123–131.
- 52 M. Monchak, T. Hupfer, A. Senyshyn, H. Boysen, D. Chernyshov, T. Hansen, K. G. Schell, E. C. Bucharsky, M. J. Hoffmann and H. Ehrenberg, *Inorg. Chem.*, 2016, **55**, 2941–2945.
- 53 A. Hayashi, K. Noi, A. Sakuda and M. Tatsumisago, *Nat. Commun.*, 2012, **3**, 856.
- 54 H.-S. Ryu, J.-S. Kim, J.-S. Park, J.-W. Park, K.-W. Kim, J.-H. Ahn, T.-H. Nam, G. Wang and H.-J. Ahn, *J. Electrochem. Soc.*, 2013, **160**, A338–A343.

